

---

# Hyperbolic Graph Diffusion Model for Molecule Generation

---

**Lingfeng Wen**

East China Normal University  
51255902043@stu.ecnu.edu.cn

**Xian Wei\***

East China Normal University  
xian.wei@tum.de

## Abstract

Recently, diffusion models have achieved remarkable performance in data generation, e.g., generating high-quality images. Nevertheless, chemistry molecules often have complex non-Euclidean spatial structures, with the behavior changing dynamically and unpredictably. Most existing diffusion models highly rely on computing the probability distribution, i.e., Gaussian distribution, in Euclidean space, which cannot capture internal non-Euclidean structures of molecules, especially the hierarchical structures of the implicit manifold surface represented by molecules. It has been observed that the complex hierarchical structures in hyperbolic embedding space become more prominent and easier to be captured. In order to leverage both the data generation power of diffusion models and the strong capability to extract complex geometric features of hyperbolic embedding, we propose to extend the diffusion model to hyperbolic manifolds for molecule generation, namely, Hyperbolic Graph Diffusion Model (HGDM). The proposed HGDM employs a hyperbolic variational autoencoder to generate the hyperbolic hidden representation of nodes and then a score-based hyperbolic graph neural network is used to learn the distribution in hyperbolic space. Numerical experimental results show that the proposed HGDM achieves higher performance on several molecular datasets, compared with state-of-the-art methods.

## 1 Introduction

Designing new molecules using deep learning models is currently an important frontier in the intersection of machine learning and chemistry. Many works use deep learning models to analyze or synthesize molecules. The molecular data used to train deep learning models mainly come in two forms: string data (such as SMILES strings)[1] and graph structure data[2]. With the research of graph representation learning, graph neural networks (GNNs) have been proven to effectively utilize the structural information of graph data[3], and the trend of using GNNs to extract molecular graph features has emerged, e.g., [2, 4, 5], fully demonstrating the significant advantage of GNNs in tasks involving molecular data and other graph structure data.

Furthermore, regarding generative models, diffusion models[6] have recently achieved amazing results in synthesizing images[7]. The diffusion model perturbs the data distribution gradually during the forward diffusion process and then learns to recover the data distribution from noise through the reverse diffusion process. The Latent Diffusion Model (LDM)[7] embeds images into a low-dimensional latent space to reduce the computational complexity. Song et al.[8] unified Score Matching with Langevin dynamics (SMLD)[9] and Denoising Diffusion Probabilistic Modeling (DDPM)[10] into a system of stochastic differential equations, referred as score-based Generative Models. GDSS[11] extended score-based Generative Models to graph generation tasks and prove that score-based models also outperform existing generative methods in molecule generation tasks.

---

\*Corresponding author

However, many real-world graphs such as protein interaction networks[12] and social networks[13, 14] often exhibit hierarchical structures. Currently, most graph neural networks operate in Euclidean space, and embedding these graphs into Euclidean space may lead to significant distortions[15]. In hyperbolic space, the circumference of a circle or the area of a sphere grows exponentially with the radius increasing[16], whereas in Euclidean space it grows polynomially. This property makes hyperbolic space well-suited for embedding hierarchical structure data[17] (See Figure1). It has been observed that the complex hierarchical structures in hyperbolic embedding space become more prominent and easier to be captured[18, 19]. Many molecular graphs also exhibit a clear tree-like structure, and some existing hyperbolic graph networks[20, 21, 22] have demonstrated superior performance in predicting molecular properties. In recent years, there have been efforts[23, 24, 25] to extend diffusion models to different manifolds in order to fully leverage the underlying structures of the data.

Inspired by LDM[7] and GDSS[11], we propose a graph diffusion model based on hyperbolic latent space. Firstly, we train a hyperbolic variational autoencoder (HVAE) to learn the hyperbolic representation of nodes, and then use a score-based Hyperbolic Graph Neural Network to learn to reverse the diffusion process in hyperbolic space. Additionally, we design a *Hyperbolic Graph Attention (HGAT)* layer as a fundamental module of HVAE and score model. Our approach effectively utilizes the properties of hyperbolic space and the generative quality advantage of the score-based model. In the molecular generation task, our method generates molecules with higher quality compared to the baseline.

Our main contributions are summarized as follows:(1) We propose a novel method for molecule generation, namely Hyperbolic Graph Diffusion Model (HGDM), which is the first attempt to combine hyperbolic methods with the graph diffusion process. In particular, we consider the molecular generation task, and experiments show that HGDM achieves better performance, especially in metrics related to structural properties. (2) We further design a novel Hyperbolic Graph Attention layer in the hyperbolic space to enhance the capability of geometrical feature extraction.

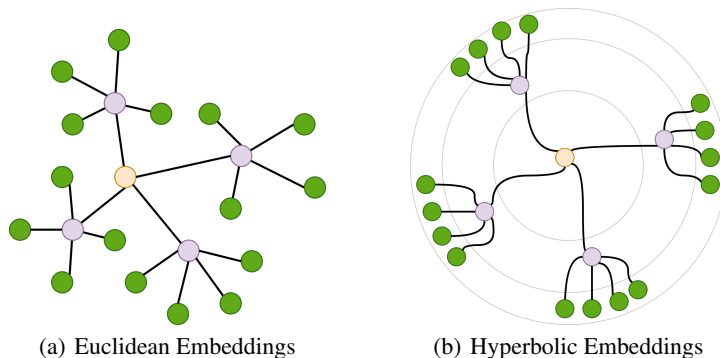


Figure 1: Given the same graph data, this figure depicts the difference between Euclidean Embeddings and Hyperbolic Embeddings.

## 2 Related Work

### 2.1 GNN for Molecule Generation

Simonovsky et al.[26] proposed a method called GraphVAE for generating small graphs using a variational autoencoder (VAE). [27] decomposes molecules into tree-shaped scaffolds of chemical functional groups and combines them with graph message passing networks to generate molecules which allows for step-by-step expansion of the molecule while maintaining chemical validity at each step. Liu et al.[28] proposed a constrained graph VAE that use masks to enforce chemical rules to improve the quality of generated molecule. [29] combines generative adversarial networks (GANs) and reinforcement learning objectives to encourage the generation of molecules with specific desired chemical properties. [30, 31] generate molecules in a flow-based fashion. [32] is an autoregressive flow-based model that utilizes discrete latent variables. Liu et al.[33] proposed an energy-based model to generate molecular graphs.

## 2.2 Hyperbolic GNN

Hyperbolic GNNs (HGNNs)[21, 34, 35, 36] utilize the characteristics of hyperbolic space to better capture the hierarchical structure in graph data. The core idea is to embed node and edge representations into hyperbolic space and use hyperbolic distance to measure their relationships, enabling better handling of graph data with a hierarchical structure, long-range dependencies, and high-dimensional correlations. In the research of hyperbolic graph neural networks, Liu et al.[21] proposed a novel GNN architecture for learning representations on hyperbolic manifolds with differentiable exponential and logarithmic mappings. The proposed architecture successfully utilizes its geometric properties to capture the hierarchical nature of the data. Chami et al.[34] introduced the Hyperbolic Graph Convolutional Network (HGCN), which achieves new state-of-the-art results in learning embeddings for real-world graphs with hierarchical and scale-free characteristics. Park et al.[37] analyzed how unsupervised tasks can benefit from learned hyperbolic representations and concluded that leveraging hyperbolic geometry can improve the performance of unsupervised tasks such as node clustering, link prediction, and image clustering. In the study of hierarchical structure in data, traditional VAEs map the data to a Euclidean latent space, which cannot effectively embed tree-like structures. Therefore, [18] endowed VAEs with a Poincaré ball model based on hyperbolic geometry as the latent space, showing better generalization to unseen data and the ability to qualitatively and quantitatively recover hierarchical structures. Subsequently, [19] learned high-quality embeddings of large taxonomies, surpassing Poincaré embeddings, especially in low dimensions, by developing an efficient Riemannian optimization method based on the Lorentz model in hyperbolic space.

## 2.3 Diffusion Models for Molecule Generation

Diffusion models[38] were generative models raised by Sohl-Dickstein et al. After the denoising diffusion probabilistic model was proposed, a large number of related works were carried out to improve this type of model such as DDIM[39], score-based diffusion[8]. Extensive work has shown that this class of new models has tremendous capabilities in the field of generation. And some methods use diffusion graph models for molecule generation. Emiel Hoogetboom et al.[40] proposed a diffusion model(EDM) for molecule generation in 3D that is equivariant to Euclidean transformations. EDM defines a noising process on both node positions and features, and learns the generative denoising process using an equivariant neural network. Minkai Xu et al.[41] proposed a novel generative model named GEODIFF for molecular conformation prediction. GEODIFF treats each atom as a particle and learns to directly reverse the diffusion process as a Markov chain. Brian L. Trippe et al.[42] proposed to learn a distribution over diverse and longer protein backbone structures via an E(3)-equivariant graph neural network. And they proved this method can achieve structurally diverse scaffolds for a fixed motif. Bowen Jing et al.[43] proposed torsional diffusion, a novel diffusion framework that operates on the space of torsion angles via a diffusion process on the hypertorus and an extrinsic-to-intrinsic score model. Compared to machine learning and cheminformatics methods, torsional diffusion generates superior conformer ensembles on a standard benchmark of drug-like molecules. It outperforms in terms of both RMSD and chemical properties, while also being orders of magnitude faster than previous diffusion-based models.

However, previous diffusion models did not take into account the geometric relationships of long ranges. The branching structure and tree-like structure of molecules are not taken into account, resulting in weak global or large-scale geometric grasping ability.

# 3 Preliminaries

## 3.1 Hyperbolic Geometry

**Riemannian Manifold.** A Riemannian manifold  $(\mathcal{M}, g^{\mathcal{M}})$  is a smooth manifold  $\mathcal{M}$  equipped with a Riemannian metric  $g^{\mathcal{M}}$  on the tangent space  $\mathcal{T}_x\mathcal{M}$  at every point  $x \in \mathcal{M}$ .  $\mathcal{T}_x\mathcal{M}$  is the vector space formed by all tangent vectors at  $x$ , which is locally a first-order approximation of the hyperbolic manifold at  $x$ . The Riemannian manifold metric  $g^{\mathcal{M}}$  assigns a positive definite inner product  $\langle \cdot, \cdot \rangle : \mathcal{T}_x\mathcal{M} \times \mathcal{T}_x\mathcal{M} \rightarrow \mathbb{R}$  on the tangent space, which makes it possible to define several geometric properties. For a curve  $\gamma : [a, b] \rightarrow \mathcal{M}$ , the length of  $\gamma$  is defined as  $L(\gamma) = \int_a^b \|\gamma'(t)\|_g dt$ , where  $\|\cdot\|_g$  denotes the norm induced by the Riemannian metric  $g^{\mathcal{M}}$ , i.e.,  $\|v\|_g = \sqrt{g(v, v)}$  for any  $v \in \mathcal{T}_x\mathcal{M}$ . A geodesic is the analogue of a straight line in Euclidean geometry, and geodesic

distance is the shortest distance between two points  $x, y$  on manifold  $\mathcal{M}$ :  $d_{\mathcal{M}}(x, y) = \inf L(\gamma)$  where  $\gamma$  is a curve that  $\gamma(a) = x, \gamma(b) = y$ . The exponential map at point  $x \in \mathcal{M}$ , denoted by  $\exp_x : T_x \mathcal{M} \rightarrow \mathcal{M}$ , takes a tangent vector  $v \in T_x \mathcal{M}$  to the point  $y \in \mathcal{M}$  obtained by "following" the geodesic starting at  $x$  in the direction of  $v$  for a unit amount of time. More precisely, if  $\gamma(t)$  is the geodesic with  $\gamma(0) = x$  and  $\gamma'(0) = v$ , then  $\exp_x(v) = \gamma_v(1) = y$ . The logarithmic map is the inverse of the exponential map  $\log_x = \exp_x^{-1} : \mathcal{M} \rightarrow T_x \mathcal{M}$ .

**Poincaré Ball Model.** Hyperbolic manifold is a Riemannian manifold with a constant negative curvature  $c$  ( $c < 0$ ). There exist multiple isomorphic hyperbolic models, like the Poincaré ball model[44], Lorentz model and Klein model. The Poincaré ball model is denoted as  $(\mathbb{B}_c^n, g_x^{\mathbb{B}})$ , where  $\mathbb{B}_c^n = \{x \in \mathbb{R}^n : \|x\|^2 < -1/c\}$  is an open  $n$ -dimensional ball with radius  $1/\sqrt{|c|}$ . Its metric tensor is  $g_x^{\mathbb{B}} = (\lambda_x^c)^2 g_x^E$ , where  $\lambda_x^c = 2/(1 + c\|x\|^2)$  is the conformal factor and  $g^E$  is the Euclidean metric, i.e.,  $\mathbf{I}_n$ . The induced distance on Poincaré ball is given by

$$d_p^c(\mathbf{x}, \mathbf{y}) = \frac{1}{\sqrt{c}} \cosh^{-1} \left( 1 + 2c \frac{\|\mathbf{x} - \mathbf{y}\|^2}{(1 - c\|\mathbf{x}\|^2)(1 - c\|\mathbf{y}\|^2)} \right), \quad (1)$$

where  $\mathbf{x}, \mathbf{y} \in B_c^n$ . [45]derived closed-form formulations for the exponential map

$$\exp_{\mathbf{z}}^c(\mathbf{v}) = \mathbf{z} \oplus_c \left( \tanh \left( \sqrt{c} \frac{\lambda_{\mathbf{z}}^c \|\mathbf{v}\|}{2} \right) \frac{\mathbf{v}}{\sqrt{c\|\mathbf{v}\|}} \right) \quad (2)$$

and the logarithm map is given by

$$\log_{\mathbf{z}}^c(\mathbf{y}) = \frac{2}{\sqrt{c}\lambda_{\mathbf{z}}^c} \tanh^{-1} \left( \sqrt{c} \|\mathbf{y} - \mathbf{z}\| \oplus_c \mathbf{y} \right) \frac{-\mathbf{z} \oplus_c \mathbf{y}}{\|\mathbf{y} - \mathbf{z}\|} \quad (3)$$

The parallel transport  $PT_{x \rightarrow y} : T_x \mathbb{B} \rightarrow T_y \mathbb{B}$  provides a way to move a vector in one tangent space to another tangent space along a curve without changing it and is given by

$$PT_{\mathbf{x} \rightarrow \mathbf{y}}^c(\mathbf{v}) = \frac{\lambda_{\mathbf{x}}^c}{\lambda_{\mathbf{y}}^c} \text{gyr}[\mathbf{y}, -\mathbf{x}] \mathbf{v} \quad (4)$$

where  $\oplus_c$  and  $\text{gyr}[\cdot, \cdot]v$  are Möbius addition[46] and gyration operator[47], respectively.

### 3.2 Graph Diffusion Model

Diffusion generative models perturb the data by adding progressively larger noise and then learn how to reverse it. Recently, Score matching with Langevin dynamics (SMLD)[9] and Denoising diffusion probabilistic modeling (DDPM)[10] are unified into the stochastic differential equation (SDE) framework[8]. The Diffusion model perturbs the data in the forward SDE and estimates the score function (that is, the gradient of the log probability density with respect to data). Sampling is performed by using the estimated score function in the reverse SDE. GDSS[11] generalizes the diffusion model to graph generation tasks. Graph diffusion models perturb both node features and adjacency matrix to learn how to convert from noise to graph.

A graph  $\mathbf{G}$  with  $N$  nodes is defined by its node features  $\mathbf{X} \in \mathbb{R}^{N \times F}$  and the weighted adjacency matrix  $\mathbf{A} \in \mathbb{R}^{N \times N}$  as  $\mathbf{G} = (\mathbf{X}, \mathbf{A}) \in \mathbb{R}^{N \times F} \times \mathbb{R}^{N \times N} := \mathcal{G}$ , where  $F$  is the dimension of the node features. Formally, the diffusion process can be represented as the trajectory of random variables  $\{\mathbf{G}_t = (\mathbf{X}_t, \mathbf{A}_t)\}_{t \in [0, T]}$  in a fixed time horizon  $[0, T]$ , where  $\mathbf{G}_0$  is a graph from the data distribution  $p_{data}$ . The SDE of diffusion process is given by:

$$d\mathbf{G}_t = \mathbf{f}_t(\mathbf{G}_t) dt + \mathbf{g}_t(\mathbf{G}_t) d\mathbf{w}, \quad \mathbf{G}_0 \sim p_{data} \quad (5)$$

where  $f_t(\cdot) : \mathcal{G} \rightarrow \mathcal{G}$  is the linear drift coefficient,  $\mathbf{g}_t(\cdot) : \mathcal{G} \rightarrow \mathcal{G} \times \mathcal{G}$  is the diffusion coefficient, and  $\mathbf{w}$  is the standard Wiener process.

the reverse-time SDE is separated into two parts in [11]:

$$\begin{cases} d\mathbf{X}_t = [\mathbf{f}_{1,t}(\mathbf{X}_t) - g_{1,t}^2 \nabla_{\mathbf{X}_t} \log p_t(\mathbf{X}_t, \mathbf{A}_t)] dt + g_{1,t} d\bar{\mathbf{w}}_1 \\ d\mathbf{A}_t = [\mathbf{f}_{2,t}(\mathbf{A}_t) - g_{2,t}^2 \nabla_{\mathbf{A}_t} \log p_t(\mathbf{X}_t, \mathbf{A}_t)] dt + g_{2,t} d\bar{\mathbf{w}}_2 \end{cases} \quad (6)$$

where  $f_{1,t}$  and  $f_{2,t}$  are linear drift coefficients satisfying  $f_t(X, A) = (f_{1,t}(X), f_{2,t}(A))$ ,  $g_{1,t}$  and  $g_{2,t}$  are scalar diffusion coefficients, and  $\bar{\mathbf{w}}_1, \bar{\mathbf{w}}_2$  are reverse-time standard Wiener processes.

## 4 The Proposed Hyperbolic Graph Diffusion Model

In this section, we introduce our novel Hyperbolic Graph Diffusion Model for molecule generation. We first introduce the Hyperbolic Wrapped Normal distribution (HWN) and how to sample from it. Then, we describe how to perturb data in the hyperbolic space following the diffusion process and our training objective. Next, we introduce a novel hyperbolic graph attention layer and the architecture of our model. Finally, we present the inverse diffusion process in the hyperbolic space.

### 4.1 Probability Distributions on Hyperbolic Space

As an alternative to the normal distribution in Euclidean space, the HWN[18, 48] is easy to sample and has a well-defined density function. For Poincaré ball manifold, which is given by:

$$\begin{aligned} \mathcal{N}_{\mathbb{B}_c^d}^W(\mathbf{z} | \boldsymbol{\mu}, \Sigma) &= \frac{d\nu^W(\mathbf{z} | \boldsymbol{\mu}, \Sigma)}{d\mathcal{M}(\mathbf{z})} \\ &= \mathcal{N}(\lambda_{\boldsymbol{\mu}}^c \log_{\boldsymbol{\mu}}(\mathbf{z}) | \mathbf{0}, \Sigma) \left( \frac{\sqrt{cd_p^c}(\boldsymbol{\mu}, \mathbf{z})}{\sinh(\sqrt{cd_p^c}(\boldsymbol{\mu}, \mathbf{z}))} \right)^{d-1}, \end{aligned} \quad (7)$$

with its log probability density function (pdf) being given by:

$$\log p(\mathbf{z}) = \log p(\mathbf{v}) - (d-1) \log \left( \frac{\sqrt{cd_p^c}(\boldsymbol{\mu}, \mathbf{z})}{\sinh(\sqrt{cd_p^c}(\boldsymbol{\mu}, \mathbf{z}))} \right), \quad (8)$$

where  $\mathbf{z} \in \mathbb{B}_c^d$ ,  $p(\mathbf{z})$  is the wrapped normal distribution and  $p(\mathbf{v})$  is the normal distribution in the tangent space of origin  $\mathcal{T}_o\mathbb{B}$ .

We use the HWN as the prior distribution on the hyperbolic manifold. This distribution can be constructed by defining Gaussian distribution on the tangent space at the origin of the hyperbolic space and projecting the distribution onto hyperbolic space after transporting the tangent space to a desired location in the space. This operation can be formalized by a combination of the parallel transport and the exponential map for the Poincaré ball model of hyperbolic space. E.g., We can sample  $\mathbf{z}$  from  $\mathcal{N}_{\mathbb{B}_c^d}^W(\boldsymbol{\mu}, \Sigma)$  by firstly sampling  $\mathbf{v} \sim \mathcal{N}(\cdot | 0, \Sigma)$  in the tangent space of origin  $\mathcal{T}_o\mathbb{B}$  then moving  $\mathbf{v}$  to  $\mathcal{T}_{\boldsymbol{\mu}}\mathbb{B}$ :  $\mathbf{u} = PT_{o \rightarrow \boldsymbol{\mu}}(\mathbf{v})$  and mapping  $\mathbf{u}$  to  $\mathbf{z} = \exp_{\boldsymbol{\mu}}^c(\mathbf{u})$

### 4.2 Perturbing Data on Hyperbolic Space

Consider two types of the disturbance of noise, Variance Exploding (VE) and Variance Preserving (VP) given in [8]. For Euclidean features, we have:

$$p_t(\mathbf{x}(t) | \mathbf{x}(0)) = \begin{cases} \mathcal{N}(\mathbf{x}(t); \mathbf{x}(0), [\sigma^2(t) - \sigma^2(0)] \mathbf{I}), & \text{(VE SDE)} \\ \mathcal{N}(\mathbf{x}(t); \mathbf{x}(0) e^{-\frac{1}{2} \int_0^t \beta(s) ds}, \mathbf{I} - \mathbf{I} e^{-\int_0^t \beta(s) ds}) & \text{(VP SDE)} \end{cases} \quad (9)$$

In order to parallelly train on different time steps, we directly give the hyperbolic version of distribution  $p(x_t | x_0)$  based on HWN:

$$p_t(\mathbf{x}(t) | \mathbf{x}(0)) = \begin{cases} \mathcal{N}_{\mathbb{B}_c^d}^W(\mathbf{x}(t); \mathbf{x}(0), [\sigma^2(t) - \sigma^2(0)] \mathbf{I}), & \text{(VE SDE)} \\ \mathcal{N}_{\mathbb{B}_c^d}^W(\mathbf{x}(t); e^{-\frac{1}{2} \int_0^t \beta(s) ds} \otimes_c \mathbf{x}(0), \mathbf{I} - \mathbf{I} e^{-\int_0^t \beta(s) ds}) & \text{(VP SDE)} \end{cases}, \quad (10)$$

where  $\otimes_c$  is the Möbius scalar multiplication[46].

### 4.3 Training Objectives

Following the GDSS[11], we train two neural networks  $\mathbf{s}_{\theta,t}$  and  $\mathbf{s}_{\phi,t}$  simultaneously to estimate the partial score functions. But differently, Given graph  $\mathbf{G} = (\mathbf{X}, \mathbf{A}) \in \mathbb{R}^{N \times F} \times \mathbb{R}^{N \times N}$  from data, we firstly use a hyperbolic variational autoencoder(HVAE) to generate the hyperbolic latent feature  $\mathbf{X}_0^B \in \mathbb{B}_c^N$  of nodes, which combine with original adjacency matrix  $\mathbf{A}$  forms  $\bar{\mathbf{G}}_0 = (\mathbf{X}_0^B, \mathbf{A}_0)$ . Then we sample  $\bar{\mathbf{G}}_t = (\mathbf{B}_t^B, \mathbf{A}_t)$  using Eq.(9) and Eq.(10).

we use  $\mathbf{s}_{\theta,t}$  and  $\mathbf{s}_{\phi,t}$  to estimate the gradients of the joint log-density so that  $\mathbf{s}_{\theta,t}(\bar{\mathbf{G}}_t) \approx \nabla_{\mathbf{X}_t^B} \log p_{0t}(\mathbf{X}_t^B | \mathbf{X}_0^B)$  and  $\mathbf{s}_{\phi,t}(\bar{\mathbf{G}}_t) \approx \nabla_{\mathbf{A}_t} \log p_{0t}(\mathbf{A}_t | \mathbf{A}_0)$ , what is worth noticing is that  $\nabla_{\mathbf{X}_t^B} \log p_{0t}(\mathbf{X}_t^B | \mathbf{X}_0^B)$  is on  $T_{\mathbf{X}_t^B}\mathbb{B}$ , which is the tangent space of  $\mathbf{X}_t^B$ .

The training objectives are given by

$$\begin{aligned} & \min_{\theta} \mathbb{E}_t \left\{ \lambda_1(t) \mathbb{E}_{\bar{\mathbf{G}}_0} \mathbb{E}_{\bar{\mathbf{G}}_t | \bar{\mathbf{G}}_0} \left\| \mathbf{s}_{\theta,t}(\bar{\mathbf{G}}_t) - \nabla_{\mathbf{X}_t^B} \log p_{0t}(\mathbf{X}_t^B | \mathbf{X}_0^B) \right\|_2^2 \right\} \\ & \min_{\phi} \mathbb{E}_t \left\{ \lambda_2(t) \mathbb{E}_{\bar{\mathbf{G}}_0} \mathbb{E}_{\bar{\mathbf{G}}_t | \bar{\mathbf{G}}_0} \left\| \mathbf{s}_{\phi,t}(\bar{\mathbf{G}}_t) - \nabla_{\mathbf{A}_t} \log p_{0t}(\mathbf{A}_t | \mathbf{A}_0) \right\|_2^2 \right\} \end{aligned} \quad (11)$$

where  $\lambda_1(t)$  and  $\lambda_2(t)$  are positive weighting functions and  $t$  is uniformly sampled from  $[0, T]$ .

In practice, we directly compute the gradient of the log-density  $\nabla_{\mathbf{X}_t^B} \log p_{0t}(\mathbf{X}_t^B | \mathbf{X}_0^B)$  using Eq.(8). However, due to the difficulty in convergence during training using this approach, we also propose two pseudo-score estimation methods, which have better loss converges during training. After perturbing the hyperbolic features using Eq.(10), the first method is to predict  $-\mathbf{v}/\sigma(t)^2$  following [9], where  $\sigma(t)$  is the standard deviation of  $p_{0t}(\mathbf{X}_t^B | \mathbf{X}_0^B)$  and  $\mathbf{v}$  is a Gaussian noise sampled from  $N(0, \sigma(t))$  in the tangent space of origin. Then, this pseudo-score is parallel transported to the tangent space of  $x_t$  using (4), which is the conventional manifold learning operation idea. However, the first method exhibits significant distortions in the direction when the curvature of the hyperbolic space deviates from zero. The second method is to predict  $\mathbf{logmap}_{\tilde{\mathbf{X}}_t^B}(\mathbf{X}_t^B)/\sigma(t)^2$  where  $\tilde{\mathbf{X}}_t^B$  is the mean of  $p_{0t}(\mathbf{X}_t^B | \mathbf{X}_0^B)$ . Empirically, we found that the second pseudo-score is consistent in direction with the true score, which can be easily understood because  $\mathbf{logmap}_{\tilde{\mathbf{X}}_t^B}(\mathbf{X}_t^B) = k\gamma'(0)$  where  $\gamma$  is the geodesic between  $\tilde{\mathbf{X}}_t^B$  and  $\mathbf{X}_t^B$ . In Table 2 and 3, we present the experimental results for these three different score computation methods. We refer to the true score estimation method as HGDM and two pseudo-score estimation methods as HGDM-PS (short for pseudo score) and HGDM-PSDC (short for pseudo score with direction corrected), respectively.

#### 4.4 Hyperbolic Graph Attention Layer

We proposed *Hyperbolic Graph Attention (HGAT)* layer as the basic building block of HVAE and the node score predicting model  $\mathbf{s}_{\theta,t}$ , which is a variant of GAT<sup>2</sup> and has smaller computational complexity than HGCN[34]. The input of our layer is a set of hyperbolic node feature  $\mathbf{h}^B = \{\mathbf{h}_1^B, \mathbf{h}_2^B, \dots, \mathbf{h}_N^B\}$ ,  $\mathbf{h}_i^B \in \mathbb{B}^d$ , where  $N$  is the number of nodes, and  $d$  is the dimension of features in each node.

We first map  $\mathbf{h}^B$  into the tangent space of origin  $T_o\mathcal{M}$  using Eq.(3) that  $\mathbf{h}^E = \log_o^c(\mathbf{h}^B)$  to perform the following attention aggregation mechanism[49]. Then We split  $\mathbf{h}^E$  into  $K$  m-dimensional features. For each node  $i$ ,  $\mathbf{h}_i^E = \|\|_{k=1}^K \mathbf{h}_i^{E,(k)}$

Next we employ multi-head attention which is similar with [49], but we add adjacent feature  $A_{ij}$  when computing attention  $e_{ij}$  coefficients where  $j \in \mathbb{N}_i$

$$e_{ij}^k = a(\mathbf{W}\mathbf{h}_i^k, \mathbf{W}\mathbf{h}_j^k, \mathbf{W}\mathbf{A}_{ij}) \quad (12)$$

We normalize them across all choices of  $j$  using the softmax function as follows:

$$\alpha_{ij}^k = \text{softmax}_j(e_{ij}^k) \quad (13)$$

then we concatenate features from  $K$  head after computing the linear combination of the features corresponding to the normalized attention coefficients.

$$\mathbf{h}'_i = \|\|_{k=1}^K \left( \sum_{j \in \mathbb{N}_i} \alpha_{ij}^k \mathbf{W}^k \mathbf{h}_j \right) \quad (14)$$

We perform the "addition" operation between the input  $\mathbf{h}_i^B$  and the output  $\mathbf{h}'_i$  of attention mechanism, which can be regarded as a residual connection[50], and finally we apply a manifold-preserving activation function  $\sigma$  (e.g., ReLU and leaky ReLU) to prevent model collapse[21].

$$\mathbf{h}_i^{B'} = \sigma(\exp_{\mathbf{h}_i^B}^c(PT_{\mathbf{o} \rightarrow \mathbf{h}_i^B}^c(\mathbf{h}'_i))) \quad (15)$$

<sup>2</sup><https://github.com/gordicaleksa/pytorch-GAT>

## 4.5 Hyperbolic Score-based Model

We implement a hyperbolic variational autoencoder to generate the hyperbolic representation  $\mathbf{X}^B$  of nodes.

**Encoder.** The encoder first utilizes a hyperbolic embedding layer to convert input feature  $\mathbf{X}^E$  of nodes into hyperbolic embeddings  $\mathbf{H}^{0,B}$ .  $(\mathbf{H}^{0,B}, \mathbf{A})$  are then put into a  $n$ -layer HGAT to learn the structural information of the graph. Then the output  $\mathbf{H}^{n,B}$  is mapped to Euclidean space using (3) and fed into an MLP to produce mean  $\mu$  and distortion  $\sigma$ .

**Decoder.** Firstly, we obtain the hyperbolic node feature  $\mathbf{X}^B = \{\mathbf{x}_1, \mathbf{x}_2, \dots, \mathbf{x}_{|V|}\}$  where each  $\mathbf{x}_i \in \mathbb{B}$  via reparametrisation mentioned in Section 4.1. Then, the decoder uses a centroid-distance layer[21] to convert  $\mathbf{X}^B$  into the Euclidean space. The centroid-distance layer is equipped with a list of learnable centroids  $\mathcal{C} = [c_1, c_2, \dots, c_{|C|}]$  where each  $c_i \in \mathbb{B}$ . By computing the pairwise distance  $\psi_{ij}$  between  $c_i$  and  $x_j$ , we obtain the euclidean features while utilizing the hyperbolic metric and use it to recover  $\mathbf{X}^E$ .

**Score Model.** We implement the hyperbolic score-based model  $s_{\theta,t}(\bar{\mathbf{G}}_t)$  to estimate  $\nabla_{\mathbf{X}_t^B} \log p_{0t}(\mathbf{X}_t^B, \mathbf{A}_t)$  as follows:

$$s_{\theta,t}(\bar{\mathbf{G}}_t) = \text{MLP} \left( \left[ \left\{ \log_{\circ}^c \left( \text{HGAT} \left( \mathbf{H}_i^B, \mathbf{A}_t \right) \right) \right\}_{i=0}^K \right] \right) \quad (16)$$

where  $\mathbf{H}_{i+1}^B = \text{HGAT}(\mathbf{H}_i^B, \mathbf{A}_t)$  with  $\mathbf{H}_0^B = \mathbf{X}_t^B$  given,  $[\cdot]$  denotes the concatenation operation, and  $K$  denotes the number of HGAT layers. We use the score-based model  $s_{\phi,t}(\bar{\mathbf{G}}_t)$  to estimate  $\nabla_{\mathbf{A}_t} \log p_{0t}(\mathbf{X}_t^B, \mathbf{A}_t)$ , which is the same with GDSS[11] as follows:

$$s_{\phi,t}(\bar{\mathbf{G}}_t) = \text{MLP} \left( \left\{ \mathbf{H}_i^E \right\}_{i=0}^K \right) \quad (17)$$

where  $\mathbf{H}_{i+1}^E = \text{GNN}(\mathbf{H}_i^E, \mathbf{A}_t)$  with  $\mathbf{H}_0^E$  obtained by a centroid-distance layer and  $L$  denotes the number of GNN layers.

## 4.6 Reversing the Diffusion Process on Hyperbolic Space

---

**Algorithm 1:** Hyperbolic PC sampling (VE SDE)

---

```

1  $x_N \sim \mathcal{N}_{\mathbb{B}_c^d}^W(0, \sigma_{max}^2 \mathbf{I})$ 
2 for  $i = N - 1$  to 0 do
3    $x'_i \leftarrow \exp_{\mathbf{x}_{i+1}}^c((\sigma_{i+1}^2 - \sigma_i^2) \mathbf{s}_{\theta}(x_{i+1}, A_{i+1}))$ 
4    $x_i \sim \mathcal{N}_{\mathbb{B}_c^d}^W(x'_i, \sqrt{\sigma_{i+1}^2 - \sigma_i^2} \mathbf{I})$ 
5   for  $j = 1$  to  $M$  do
6      $x''_i \leftarrow \epsilon_i \exp_{\mathbf{x}_i}^c(\epsilon_i \mathbf{s}_{\theta}(x_i, A_i))$ 
7      $x_i \sim \mathcal{N}_{\mathbb{B}_c^d}^W(x''_i, \sqrt{2\epsilon_i} \mathbf{I})$ 
8   end
9 end
10 return  $x_0$ 
```

---



---

**Algorithm 2:** Hyperbolic PC sampling (VP SDE)

---

```

1  $x_N \sim \mathcal{N}_{\mathbb{B}_c^d}^W(0, \mathbf{I})$ 
2 for  $i = N - 1$  to 0 do
3    $x'_i \leftarrow (2 - \sqrt{1 - \beta_{i+1}}) \otimes_c \mathbf{x}_{i+1}$ 
4    $x''_i \leftarrow \exp_{\mathbf{x}_i}^c(\beta_{i+1} \mathbf{s}_{\theta}(x_{i+1}, A_{i+1}))$ 
5    $x_i \sim \mathcal{N}_{\mathbb{B}_c^d}^W(x'_i, \sqrt{\beta_{i+1}} \mathbf{I})$ 
6   for  $j = 1$  to  $M$  do
7      $x''_i \leftarrow \epsilon_i \exp_{\mathbf{x}_i}^c(\epsilon_i \mathbf{s}_{\theta}(x_i, A_i))$ 
8      $x_i \sim \mathcal{N}_{\mathbb{B}_c^d}^W(x''_i, \sqrt{2\epsilon_i} \mathbf{I})$ 
9   end
10 end
11 return  $x_0$ 
```

---

We implement the Predictor-Corrector samplers[8] in hyperbolic space(see Algorithms 1 and 2), where we use the Möbius scalar multiplication  $\otimes_c$ [46] to replace the euclidean scalar multiplication operation and use the exponential map Eq.(2) to implement the "addition" operation between tangent vectors and hyperbolic vectors. After sampling, a pre-trained decoder from HVAE is used to recover  $x_0$  back into the original node features, such as atom types.

Table 1: Statistics of QM9 and ZINC250k datasets used in the molecule generation tasks.

Dataset	Number of graphs	Number of nodes	Number of node types	Number of edge types
QM9	133,885	$1 \leq  V  \leq 9$	4	3
ZINC250k	249,455	$6 \leq  V  \leq 38$	9	3

Table 2: Generation results on the QM9 dataset. Results of the baselines are taken from [11]

	Method	Validity w/o correction (%) $\uparrow$	NSPDK MMD $\downarrow$	FCD $\downarrow$	Validity (%) $\uparrow$	Uniqueness (%) $\uparrow$	Novelty (%) $\uparrow$
Autoreg.	GraphDF+FC	67	0.020	5.268	<b>100.00</b>	94.51	88.83
	GraphDF+FC	74.43	0.021	5.625	<b>100.00</b>	88.64	86.59
	GraphDF	82.67	0.063	10.816	<b>100.00</b>	97.62	98.10
	GraphDF+FC	93.88	0.064	10.928	<b>100.00</b>	98.58	<b>98.54</b>
One-shot	MoFlow	91.36	0.017	4.467	<b>100.00</b>	98.65	94.72
	EDP-GNN	47.52	0.005	<b>2.680</b>	<b>100.00</b>	<b>99.25</b>	86.58
	GraphEBM	8.22	0.030	6.143	<b>100.00</b>	97.90	97.01
	GDSS	95.72	0.003	2.900	<b>100.00</b>	98.46	86.27
One-shot	HGDM+PS (ours)	88.51	0.009	3.914	<b>100.00</b>	94.28	88.77
	HGDM+PSDC (ours)	78.29	0.004	3.427	<b>100.00</b>	97.77	80.91
	HGDM (ours)	<b>96.39</b>	<b>0.002</b>	3.254	<b>100.00</b>	99.17	82.47

## 5 Experiments

In this section, we evaluate our method on molecular datasets and compare it with the baselines.

### 5.1 Molecule Generation

**Datasets** Following the GDSS[11], we tested our model on the QM9[51] and ZINC250[52] datasets to assess its ability to learn molecular distributions. QM9 dataset is a comprehensive dataset that provides molecular properties for small organic molecules. The database contains 134k stable organic molecules with up to 9 heavy atoms (CONF). ZINC250k datasets encompass a total of 250k chemical compounds with drug-like properties. On average, these molecules are characterized by a larger size (with an average of 23 heavy atoms) and possess greater structural complexity when compared to the molecules in QM9. Following previous works[11, 30, 32], the molecules are kekulized by the RDKit library[53] with hydrogen atoms removed. The statistics of the 2 datasets are given in Table 1.

**Metrics** We sample 10,000 molecules using our model and evaluate their quality with the following metrics. Fréchet ChemNet Distance (FCD)[54] evaluates the distance between the training sets and generated sets by analyzing the activations of the penultimate layer of the ChemNet. Neighborhood Subgraph Pairwise Distance Kernel (NSPDK) MMD[55] computes MMD between the generated molecules and test molecules while considering both node and edge features for evaluation. It is important to note that FCD and NSPDK MMD are crucial metrics that evaluate the ability to learn the distribution of the training molecules by measuring the proximity of the generated molecules to the distribution. Specifically, FCD assesses the ability in the context of chemical space, whereas NSPDK MMD measures the ability in terms of the graph structure. Validity w/o correction, we used for fair comparing with [11], is the proportion of valid molecules without valency correction or edge resampling.

**Baselines** We use GDSS[11] as our main baseline. Moreover, We compare the performance of HGDM against GraphAF[30], MoFlow[31], GraphDF[32] and GraphEBM[33]. Our Baselines also include 2 variants (GraphAF+FC and GraphDF+FC) of GraphAF and GraphDF which are mentioned in [11].

**Results** Table 2 shows that the proposed HGDM achieves the highest validity without using the post-hoc valency correction. This indicates that the HGDM can learn the dependencies between nodes and edges from the hyperbolic latent space and get benefits from it. HGDM also outperforms all the baselines in NSPDK MMD, which shows that HGDM effectively learns the distribution of graph structure. Our method also achieves comparable results in the rest of metrics. We find that the molecules generated by HGDM have a lower novelty. This can be interpreted that novelty may not be



Table 3: **Generation results on the ZINC250k dataset.** Results of the baselines are taken from [11]

	Method	Validity w/o correction (%) $\uparrow$	NSPDK MMD $\downarrow$	FCD $\downarrow$	Validity (%) $\uparrow$	Uniqueness (%) $\uparrow$	Novelty (%) $\uparrow$
Autoreg.	GraphDF+FC	68	0.044	16.289	<b>100.00</b>	99.10	<b>100.00</b>
	GraphDF+FC	68.47	0.044	16.023	<b>100.00</b>	98.64	99.99
	GraphDF	89.03	0.176	34.202	<b>100.00</b>	99.16	<b>100.00</b>
	GraphDF+FC	90.61	0.177	33.546	<b>100.00</b>	99.63	<b>100.00</b>
One-shot	MoFlow	63.11	0.046	20.931	<b>100.00</b>	99.99	<b>100.00</b>
	EDP-GNN	82.97	0.049	16.737	<b>100.00</b>	99.79	<b>100.00</b>
	GraphEBM	5.29	0.212	35.471	99.96	98.79	<b>100.00</b>
	GDSS	<b>97.01</b>	0.019	<b>14.656</b>	<b>100.00</b>	99.64	<b>100.00</b>
One-shot	HGDM+PS (ours)	87.10	0.021	19.70	<b>100.00</b>	<b>100.00</b>	<b>100.00</b>
	HGDM+PSDC (ours)	77.4	<b>0.017</b>	18.18	<b>100.00</b>	<b>100.00</b>	<b>100.00</b>
	HGDM (ours)	82.50	0.031	22.59	<b>100.00</b>	99.99	<b>100.00</b>

Table 4: **Generation results of the variants of GDSS on the QM9 dataset.**

	Validity w/o correction (%) $\uparrow$	NSPDK MMD $\downarrow$	FCD $\downarrow$	Validity (%) $\uparrow$	Uniqueness (%) $\uparrow$	Novelty (%) $\uparrow$
GDSS+AE	95.95	0.003	<b>2.615</b>	<b>100.00</b>	97.75	81.38
HGDM (ours)	<b>96.39</b>	<b>0.002</b>	3.254	<b>100.00</b>	<b>99.17</b>	<b>82.47</b>

an indicator of good performance because QM9 is an enumeration of all possible molecules up to 9 heavy atoms that satisfy a predefined set of constraints, as discussed in [56, 57]. Comparing the two variants of HGDM, we find that HGDM+PSDC achieves better NSPDK MMD and FCD, proving that maintaining the correct direction in sampling is crucial.

We also report the generation results of ZINC250 in Table 3. We find that HGDM does not outperform GDSS, which is the counterpart of our model in Euclidean space. This is probably because molecules in ZINC250 are more complex in structure compared to those in QM9, this makes HGDM more unstable in predicting the true score. We also observed that molecules in ZINC exhibit a higher frequency of ring structures, which reduces their potential tree-like structures. However, the variants of our model HGDM+PSDC perform well in NSPDK MMD, which means that HGDM can effectively capture the structural information under the condition of good convergence.

## 5.2 Ablation Study

We implement a variant of GDSS called GDSS+AE, which incorporates an autoencoder to generate the Euclidean embedding of nodes and uses GDSS to estimate the score function in Euclidean latent space. We use GDSS+AE to exclude potential interference from additional autoencoder in assessing the effectiveness of the hyperbolic methods. The results of our proposed method HGDM and GDSS+AE in QM9 are reported in 4. We observe that HGDM outperforms the GDSS+AE on most metrics, except for FCD, which can suggest that the hyperbolic method is helpful for the generation of data with a hierarchical structure.

## 6 Conclusion

In this paper, we introduce the hyperbolic manifold and the normal distribution in the hyperbolic space. We propose a two-stage Hyperbolic Graph Diffusion Model (HGDM) to better learn the distribution of hierarchically structured data. HGDM consists of a hyperbolic variational autoencoder(HVAE) and a hyperbolic score model, where the HVAE generates the hyperbolic representation of nodes, and the hyperbolic score model learns the data distribution in the hyperbolic space. We also introduce the diffusion and inverse diffusion processes in the hyperbolic space. Empirically, we found that learning the distribution in the hyperbolic space is beneficial for the quality of generated data if the data has a hierarchical structure. Experimental results in molecule generation show that HGDM achieves competitive results compared to state-of-the-art graph score-based models.

## References

- [1] Marwin HS Segler, Thierry Kogej, Christian Tyrchan, and Mark P Waller. Generating focused molecule libraries for drug discovery with recurrent neural networks. *ACS central science*, 4(1):120–131, 2018.
- [2] David K Duvenaud, Dougal Maclaurin, Jorge Iparraguirre, Rafael Bombarell, Timothy Hirzel, Alán Aspuru-Guzik, and Ryan P Adams. Convolutional networks on graphs for learning molecular fingerprints. *Advances in neural information processing systems*, 28, 2015.
- [3] Nima Dehmamy, Albert-László Barabási, and Rose Yu. Understanding the representation power of graph neural networks in learning graph topology. *Advances in Neural Information Processing Systems*, 32, 2019.
- [4] Kristof Schütt, Pieter-Jan Kindermans, Huziel Enoc Saucedo Felix, Stefan Chmiela, Alexandre Tkatchenko, and Klaus-Robert Müller. Schnet: A continuous-filter convolutional neural network for modeling quantum interactions. *Advances in neural information processing systems*, 30, 2017.
- [5] Zhuoran Qiao, Matthew Welborn, Animashree Anandkumar, Frederick R Manby, and Thomas F Miller III. Orbnet: Deep learning for quantum chemistry using symmetry-adapted atomic-orbital features. *The Journal of chemical physics*, 153(12):124111, 2020.
- [6] Jascha Sohl-Dickstein, Eric Weiss, Niru Maheswaranathan, and Surya Ganguli. Deep unsupervised learning using nonequilibrium thermodynamics. In *International Conference on Machine Learning*, pages 2256–2265. PMLR, 2015.
- [7] Robin Rombach, Andreas Blattmann, Dominik Lorenz, Patrick Esser, and Björn Ommer. High-resolution image synthesis with latent diffusion models. In *Proceedings of the IEEE/CVF Conference on Computer Vision and Pattern Recognition*, pages 10684–10695, 2022.
- [8] Yang Song, Jascha Sohl-Dickstein, Diederik P Kingma, Abhishek Kumar, Stefano Ermon, and Ben Poole. Score-based generative modeling through stochastic differential equations. *arXiv preprint arXiv:2011.13456*, 2020.
- [9] Yang Song and Stefano Ermon. Generative modeling by estimating gradients of the data distribution. *Advances in neural information processing systems*, 32, 2019.
- [10] Jonathan Ho, Ajay Jain, and Pieter Abbeel. Denoising diffusion probabilistic models. *Advances in Neural Information Processing Systems*, 33:6840–6851, 2020.
- [11] Jaehyeong Jo, Seul Lee, and Sung Ju Hwang. Score-based generative modeling of graphs via the system of stochastic differential equations. In *International Conference on Machine Learning*, pages 10362–10383. PMLR, 2022.
- [12] Alexei Vázquez, Alessandro Flammini, Amos Maritan, and Alessandro Vespignani. Modeling of protein interaction networks. *Complexus*, 1(1):38–44, 2003.
- [13] Cheng Yang, Maosong Sun, Wayne Xin Zhao, Zhiyuan Liu, and Edward Y Chang. A neural network approach to jointly modeling social networks and mobile trajectories. *ACM Transactions on Information Systems (TOIS)*, 35(4):1–28, 2017.
- [14] Wenqi Fan, Yao Ma, Qing Li, Yuan He, Eric Zhao, Jiliang Tang, and Dawei Yin. Graph neural networks for social recommendation. In *The world wide web conference*, pages 417–426, 2019.
- [15] Nathan Linial, Eran London, and Yuri Rabinovich. The geometry of graphs and some of its algorithmic applications. *Combinatorica*, 15:215–245, 1995.
- [16] Tamara Munzner. H3: Laying out large directed graphs in 3d hyperbolic space. In *Proceedings of VIZ'97: Visualization Conference, Information Visualization Symposium and Parallel Rendering Symposium*, pages 2–10. IEEE, 1997.
- [17] Frederic Sala, Chris De Sa, Albert Gu, and Christopher Ré. Representation tradeoffs for hyperbolic embeddings. In *International conference on machine learning*, pages 4460–4469. PMLR, 2018.
- [18] Emile Mathieu, Charline Le Lan, Chris J Maddison, Ryota Tomioka, and Yee Whye Teh. Continuous hierarchical representations with poincaré variational auto-encoders. *Advances in neural information processing systems*, 32, 2019.

- [19] Maximillian Nickel and Douwe Kiela. Learning continuous hierarchies in the lorentz model of hyperbolic geometry. In *International conference on machine learning*, pages 3779–3788. PMLR, 2018.
- [20] Zhenxing Wu, Dejun Jiang, Chang-Yu Hsieh, Guangyong Chen, Ben Liao, Dongsheng Cao, and Tingjun Hou. Hyperbolic relational graph convolution networks plus: a simple but highly efficient qsar-modeling method. *Briefings in Bioinformatics*, 22(5):bbab112, 2021.
- [21] Qi Liu, Maximilian Nickel, and Douwe Kiela. Hyperbolic graph neural networks. *Advances in neural information processing systems*, 32, 2019.
- [22] Ke Yu, Shyam Visweswaran, and Kayhan Batmanghelich. Semi-supervised hierarchical drug embedding in hyperbolic space. *Journal of chemical information and modeling*, 60(12):5647–5657, 2020.
- [23] Chin-Wei Huang, Milad Aghajohari, Joey Bose, Prakash Panangaden, and Aaron C Courville. Riemannian diffusion models. *Advances in Neural Information Processing Systems*, 35:2750–2761, 2022.
- [24] Valentin De Bortoli, Emile Mathieu, Michael Hutchinson, James Thornton, Yee Whye Teh, and Arnaud Doucet. Riemannian score-based generative modeling. *arXiv preprint arXiv:2202.02763*, 2022.
- [25] Bowen Jing, Gabriele Corso, Jeffrey Chang, Regina Barzilay, and Tommi Jaakkola. Torsional diffusion for molecular conformer generation. *arXiv preprint arXiv:2206.01729*, 2022.
- [26] Martin Simonovsky and Nikos Komodakis. Graphvae: Towards generation of small graphs using variational autoencoders. In *Artificial Neural Networks and Machine Learning–ICANN 2018: 27th International Conference on Artificial Neural Networks, Rhodes, Greece, October 4-7, 2018, Proceedings, Part I 27*, pages 412–422. Springer, 2018.
- [27] Wengong Jin, Regina Barzilay, and Tommi Jaakkola. Junction tree variational autoencoder for molecular graph generation. In *International conference on machine learning*, pages 2323–2332. PMLR, 2018.
- [28] Qi Liu, Miltiadis Allamanis, Marc Brockschmidt, and Alexander Gaunt. Constrained graph variational autoencoders for molecule design. *Advances in neural information processing systems*, 31, 2018.
- [29] Nicola De Cao and Thomas Kipf. Molgan: An implicit generative model for small molecular graphs. *arXiv preprint arXiv:1805.11973*, 2018.
- [30] Chence Shi, Minkai Xu, Zhaocheng Zhu, Weinan Zhang, Ming Zhang, and Jian Tang. Graphaf: a flow-based autoregressive model for molecular graph generation. *arXiv preprint arXiv:2001.09382*, 2020.
- [31] Chengxi Zang and Fei Wang. Moflow: an invertible flow model for generating molecular graphs. In *Proceedings of the 26th ACM SIGKDD International Conference on Knowledge Discovery & Data Mining*, pages 617–626, 2020.
- [32] Youzhi Luo, Keqiang Yan, and Shuiwang Ji. Graphdf: A discrete flow model for molecular graph generation. In *International Conference on Machine Learning*, pages 7192–7203. PMLR, 2021.
- [33] Meng Liu, Keqiang Yan, Bora Oztekin, and Shuiwang Ji. Graphebm: Molecular graph generation with energy-based models. *arXiv preprint arXiv:2102.00546*, 2021.
- [34] Ines Chami, Zhitao Ying, Christopher Ré, and Jure Leskovec. Hyperbolic graph convolutional neural networks. *Advances in neural information processing systems*, 32, 2019.
- [35] Jindou Dai, Yuwei Wu, Zhi Gao, and Yunde Jia. A hyperbolic-to-hyperbolic graph convolutional network. In *Proceedings of the IEEE/CVF Conference on Computer Vision and Pattern Recognition*, pages 154–163, 2021.
- [36] Weize Chen, Xu Han, Yankai Lin, Hexu Zhao, Zhiyuan Liu, Peng Li, Maosong Sun, and Jie Zhou. Fully hyperbolic neural networks. *arXiv preprint arXiv:2105.14686*, 2021.
- [37] Jiwoong Park, Junho Cho, Hyung Jin Chang, and Jin Young Choi. Unsupervised hyperbolic representation learning via message passing auto-encoders. In *Proceedings of the IEEE/CVF Conference on Computer Vision and Pattern Recognition*, pages 5516–5526, 2021.

- [38] Jascha Sohl-Dickstein, Eric Weiss, Niru Maheswaranathan, and Surya Ganguli. Deep unsupervised learning using nonequilibrium thermodynamics. pages 2256–2265, 2015.
- [39] Stefano Ermon Jiaming Song, Chenlin Meng. Denoising diffusion implicit models. *arXiv preprint arXiv:2010.02502*, 2020.
- [40] Emiel Hoogeboom, Víctor Garcia Satorras, Clément Vignac, and Max Welling. Equivariant diffusion for molecule generation in 3d. pages 8867–8887, 2022.
- [41] Minkai Xu, Lantao Yu, Yang Song, Chence Shi, Stefano Ermon, and Jian Tang. Geodiff: a geometric diffusion model for molecular conformation generation. *arXiv preprint arXiv:2203.02923*, 2022.
- [42] Brian L. Trippe, Jason Yim, Doug Tischer, David Baker, Tamara Broderick, Regina Barzilay, and Tommi Jaakkola. Diffusion probabilistic modeling of protein backbones in 3d for the motif-scaffolding problem. *arXiv preprint arXiv:2206.04119*, 2022.
- [43] Bowen Jing, Gabriele Corso, Jeffrey Chang, Regina Barzilay, and Tommi Jaakkola. Torsional diffusion for molecular conformer generation. *arXiv preprint arXiv:2206.01729*, 2022.
- [44] Eugenio Beltrami. *Teoria fondamentale degli spazii di curvatura costante: memoria*. F. Zanetti, 1868.
- [45] Octavian Ganea, Gary Bécigneul, and Thomas Hofmann. Hyperbolic neural networks. *Advances in neural information processing systems*, 31, 2018.
- [46] Abraham A Ungar. The hyperbolic square and mobius transformations. *Banach Journal of Mathematical Analysis*, 1(1):101–116, 2007.
- [47] Abraham Albert Ungar. A gyrovector space approach to hyperbolic geometry. *Synthesis Lectures on Mathematics and Statistics*, 1(1):1–194, 2008.
- [48] Yoshihiro Nagano, Shoichiro Yamaguchi, Yasuhiro Fujita, and Masanori Koyama. A wrapped normal distribution on hyperbolic space for gradient-based learning. In *International Conference on Machine Learning*, pages 4693–4702. PMLR, 2019.
- [49] Petar Veličković, Guillem Cucurull, Arantxa Casanova, Adriana Romero, Pietro Lio, and Yoshua Bengio. Graph attention networks. *arXiv preprint arXiv:1710.10903*, 2017.
- [50] Kaiming He, Xiangyu Zhang, Shaoqing Ren, and Jian Sun. Deep residual learning for image recognition. In *Proceedings of the IEEE conference on computer vision and pattern recognition*, pages 770–778, 2016.
- [51] Raghunathan Ramakrishnan, Pavlo O Dral, Matthias Rupp, and O Anatole Von Lilienfeld. Quantum chemistry structures and properties of 134 kilo molecules. *Scientific data*, 1(1):1–7, 2014.
- [52] John J Irwin, Teague Sterling, Michael M Mysinger, Erin S Bolstad, and Ryan G Coleman. Zinc: a free tool to discover chemistry for biology. *Journal of chemical information and modeling*, 52(7):1757–1768, 2012.
- [53] Greg Landrum et al. Rdkit: Open-source cheminformatics software. 2016. URL <http://www.rdkit.org/>, <https://github.com/rdkit/rdkit>, 149(150):650, 2016.
- [54] Kristina Preuer, Philipp Renz, Thomas Unterthiner, Sepp Hochreiter, and Gunter Klambauer. Fréchet chemnet distance: a metric for generative models for molecules in drug discovery. *Journal of chemical information and modeling*, 58(9):1736–1741, 2018.
- [55] Fabrizio Costa and Kurt De Grave. Fast neighborhood subgraph pairwise distance kernel. In *Proceedings of the 26th International Conference on Machine Learning*, pages 255–262. Omnipress; Madison, WI, USA, 2010.
- [56] Clement Vignac and Pascal Frossard. Top-n: Equivariant set and graph generation without exchangeability. *arXiv preprint arXiv:2110.02096*, 2021.
- [57] Emiel Hoogeboom, Victor Garcia Satorras, Clément Vignac, and Max Welling. Equivariant diffusion for molecule generation in 3d. In *International Conference on Machine Learning*, pages 8867–8887. PMLR, 2022.
- [58] Prithviraj Sen, Galileo Namata, Mustafa Bilgic, Lise Getoor, Brian Galligher, and Tina Eliassi-Rad. Collective classification in network data. *AI magazine*, 29(3):93–93, 2008.

- [59] Ida Schomburg, Antje Chang, Christian Ebeling, Marion Gremse, Christian Heldt, Gregor Huhn, and Dietmar Schomburg. Brenda, the enzyme database: updates and major new developments. *Nucleic acids research*, 32(suppl\_1):D431–D433, 2004.
- [60] Yujia Li, Oriol Vinyals, Chris Dyer, Razvan Pascanu, and Peter Battaglia. Learning deep generative models of graphs. *arXiv preprint arXiv:1803.03324*, 2018.
- [61] Jiaxuan You, Rex Ying, Xiang Ren, William Hamilton, and Jure Leskovec. Graphrnn: Generating realistic graphs with deep auto-regressive models. In *International conference on machine learning*, pages 5708–5717. PMLR, 2018.
- [62] Jenny Liu, Aviral Kumar, Jimmy Ba, Jamie Kiros, and Kevin Swersky. Graph normalizing flows. *Advances in Neural Information Processing Systems*, 32, 2019.
- [63] Chenhao Niu, Yang Song, Jiaming Song, Shengjia Zhao, Aditya Grover, and Stefano Ermon. Permutation invariant graph generation via score-based generative modeling. In *International Conference on Artificial Intelligence and Statistics*, pages 4474–4484. PMLR, 2020.
- [64] Gary Bécigneul and Octavian-Eugen Ganea. Riemannian adaptive optimization methods. *arXiv preprint arXiv:1810.00760*, 2018.
- [65] Max Kochurov, Rasul Karimov, and Serge Kozlukov. Geoopt: Riemannian optimization in pytorch. *arXiv preprint arXiv:2005.02819*, 2020.
- [66] Adam Paszke, Sam Gross, Francisco Massa, Adam Lerer, James Bradbury, Gregory Chanan, Trevor Killeen, Zeming Lin, Natalia Gimelshein, Luca Antiga, et al. Pytorch: An imperative style, high-performance deep learning library. *Advances in neural information processing systems*, 32, 2019.

Table 5: **Generation results on the generic graph datasets.** Results of the baselines are taken from [11]. Hyphen (-) denotes the results are not provided in the original paper. The best results are highlighted in bold (the smaller the better).

		Ego-small				Community-small				Enzymes				Grid			
		Real, $4 \leq  V  \leq 18$				Synthetic, $12 \leq  V  \leq 20$				Real, $10 \leq  V  \leq 125$				Synthetic, $100 \leq  V  \leq 400$			
		Deg.	Clus.	Orbit	Avg.	Deg.	Clus.	Orbit	Avg.	Deg.	Clus.	Orbit	Avg.	Deg.	Clus.	Orbit	Avg.
Autoreg.	DeepGMG	0.040	0.100	0.020	0.053	0.220	0.950	0.400	0.523	-	-	-	-	-	-	-	-
	GraphRNN	0.090	0.220	0.003	0.104	0.080	0.120	0.040	0.080	<b>0.017</b>	0.062	0.046	0.042	<b>0.064</b>	0.043	<b>0.021</b>	<b>0.043</b>
	GraphAF	0.03	0.11	<b>0.001</b>	0.047	0.18	0.20	0.02	0.133	1.669	1.283	0.266	1.073	-	-	-	-
	GraphDF	0.04	0.13	0.01	0.060	0.06	0.12	0.03	0.070	1.503	1.061	0.202	0.922	-	-	-	-
One-shot	GraphVAE	0.130	0.170	0.050	0.117	0.350	0.980	0.540	0.623	1.369	0.629	0.191	0.730	1.619	<b>0.0</b>	0.919	0.846
	GNF	0.030	0.100	<b>0.001</b>	0.044	0.200	0.200	0.110	0.170	-	-	-	-	-	-	-	-
	EDP-GNN	0.052	0.093	0.007	0.051	0.053	0.144	0.026	0.074	0.023	0.268	0.082	0.124	0.455	0.238	0.328	0.340
	GDSS	<b>0.021</b>	<b>0.024</b>	0.007	<b>0.017</b>	0.045	<b>0.086</b>	<b>0.007</b>	<b>0.046</b>	0.026	<b>0.061</b>	<b>0.009</b>	<b>0.032</b>	0.111	0.005	0.070	0.062
	HGDM (ours)	<b>0.021</b>	0.035	0.006	0.021	<b>0.019</b>	0.104	0.024	0.049	0.673	0.290	0.058	0.340	0.920	0.015	0.149	0.361

## A Additional Experimental Results

In this section, we provide additional experimental results for the generic graph generation tasks.

**Experimental Setup** We validate HGDM on four generic graph datasets: (1) Ego-small, 200 small ego graphs drawn from larger Citeseer network dataset[58], (2) Community-small, 100 randomly generated community graphs[11], (3) Enzymes, 587 protein graphs which represent the protein tertiary structures of the enzymes from the BRENDA database[59], and (4) Grid, 100 standard 2D grid graphs[11]. We use the maximum mean discrepancy (MMD) to compare the distributions of graph statistics between the same number of generated and test graphs. Following Jo et al.[11], we measure the distributions of degree, clustering coefficient, and the number of occurrences of orbits with 4 nodes.

**Baselines** We compare our proposed method against the following deep generative models. GraphVAE[26] is a one-shot VAE-based model. DeepGMG[60] and GraphRNN[61] are autoregressive RNNbased models. GNF[62] is a one-shot flow-based model. GraphAF[30] is an autoregressive flow-based model. EDP-GNN[63] and GDSS[11] are one-shot score-based models. GraphDF[32] is an autoregressive flow-based model that utilizes discrete latent variables.

**Results** Table 5 shows that our HGDM achieves competitive performance to GDSS and outperforms other baselines on small graph generation, e.g., Ego-small and Community-small. This means that HGDM can effectively learn hyperbolic distributions from data with a hierarchical structure. However, for Enzymes and Grid, the graphs in these datasets deviate more from the tree-like structure and the HGDM does not perform better than its Euclidean counterpart, i.e. GDSS. We visualize the generated graphs of HGDM in Appendix C.2.

## B Experimental Details

In this section, we explain the details of the experiments including the generic graph generation tasks, and the molecule generation tasks. We describe the implementation details of HGDM and further provide the hyperparameters used in the experiments in Table 6. For fair comparison, we keep most of the hyperparameters consistent with GDSS[11].

### B.1 Molecule Generation

Following Jo et al.[11], Each molecule is preprocessed into a graph with the node features  $X \in \{0, 1\}^{N \times F}$  and the adjacency matrix  $A \in \{0, 1, 2, 3\}^{N \times N}$ , where  $N$  is the maximum number of atoms in a molecule of the dataset, and  $F$  is the number of atom types. The entries of A indicate the bond types. We kekulize the molecules using the RDKit library[53] and remove all hydrogen atoms following the standard procedure[30, 32]. We make use of the valency correction proposed by Zang et al.[31]. We perform the grid search to choose the best signal-to-noise ratio (SNR) in  $\{0.1, 0.2, 0.3, 0.4, 0.5, 0.6, 0.7, 0.8, 0.9, 1.0\}$  and the scale coefficient in  $\{0.1, 0.2, 0.3, 0.4, 0.5, 0.6, 0.7, 0.8, 0.9, 1.0\}$ . Considering the variation brought by hyperbolic space, we use different SNR and scale coefficients for X and A in molecular sampling, which is different from GDSS[11]. We choose the hyperparameters that exhibit the best FCD value among those which show the novelty that exceeds

Table 6: **Hyperparameters of HGDM** used in the generic graph generation tasks and the molecule generation tasks. We provide the hyperparameters of the score-based models ( $s_\theta$  and  $s_\phi$ ), the diffusion processes (SDE for X and A), the SDE solver, and the training.

Hyperparameter		Ego-small	Community-small	Enzymes	Grid	QM9	ZINC250k
$s_\theta$	Number of HGAT layers	2	3	5	5	2	2
	Hidden dimension	32	32	32	32	16	16
$s_\phi$	Number of attention heads	4	4	4	4	4	4
	Number of initial channels	2	2	2	2	2	2
	Number of hidden channels	8	8	8	8	8	8
	Number of final channels	4	4	4	4	4	4
	Number of GCN layers	5	5	7	7	3	6
	Hidden dimension	32	32	32	32	16	16
SDE for X	Type	VP	VP	VE	VP	VE	VP
	Number of sampling steps	1000	1000	1000	1000	1000	1000
	$\beta_{min}$	0.1	0.1	0.1	0.1	0.1	0.1
	$\beta_{max}$	4.0	2.0	2.0	4.0	2.0	4.0
SDE for A	Type	VP	VP	VE	VP	VE	VE
	Number of sampling steps	1000	1000	1000	1000	1000	1000
	$\beta_{min}$	0.1	0.1	0.2	0.2	0.1	0.2
	$\beta_{max}$	1.0	1.0	1.0	0.8	1.0	1.0
Solver	Type	Rev. + Langevin	EM + Langevin	Rev. + Langevin	Rev. + Langevin	Rev. + Langevin	Rev. + Langevin
	SNR for X	0.05	0.2	0.05	0.05	1.0	0.4
	Scale coefficient for X	1.0	1.0	1.0	1.0	0.9	0.6
	SNR for A	0.05	0.2	0.05	0.05	0.2	0.2
	Scale coefficient for A	1.0	1.0	1.0	1.0	0.7	0.9
Train	Optimizer	Riemannian Adam	Riemannian Adam	Riemannian Adam	Riemannian Adam	Riemannian Adam	Riemannian Adam
	Learning rate	$1 \times 10^{-2}$	$1 \times 10^{-2}$	$1 \times 10^{-2}$	$1 \times 10^{-2}$	$5 \times 10^{-3}$	$5 \times 10^{-3}$
	Weight decay	$1 \times 10^{-4}$	$1 \times 10^{-4}$	$1 \times 10^{-4}$	$1 \times 10^{-4}$	$1 \times 10^{-4}$	$1 \times 10^{-4}$
	Batch size	128	128	64	8	1024	1024
	Number of epochs	5000	5000	5000	5000	300	500

80%. After generating the samples by simulating the reverse diffusion process, we quantize the entries of the adjacency matrices to  $\{0, 1, 2, 3\}$  by clipping the values as:  $(-\infty, 0.5)$  to 0, the values of  $[0.5, 1.5)$  to 1, the values of  $[1.5, 2.5)$  to 2, and the values of  $[2.5, +\infty)$  to 3. We use a hyperbolic variational autoencoder (HVAE) to generate the hyperbolic node features. For all experiments, the encoder equips 3 *Hyperbolic Graph Attention (HGAT)* layers, and the decoder is a centroid-distance layer[21] followed by a shallow multilayer perceptron (MLP). We fix the curvature of the hyperbolic space to -0.01, which empirically improves performance. For score model  $s_\theta$ , we use HGAT layers to replace the GCN layers in GDSS[11]. We optimize our model with Riemannian Adam[64, 65]. We report the remaining hyperparameters used in the experiment in Table 6.

## B.2 Generic Graph Generation

For a fair evaluation of the generic graph generation task, we follow the standard setting of existing works[11, 61, 62, 63] from the node features to the data splitting. For HGDM, we initialize the node features as the one-hot encoding of the degrees. We perform the grid search to choose the best signal-to-noise ratio (SNR) in  $\{0.05, 0.1, 0.15, 0.2\}$  and the scale coefficient in the  $\{0.1, 0.2, 0.3, 0.4, 0.5, 0.6, 0.7, 0.8, 0.9, 1.0\}$ . We select the best results with the lowest average of degree, clustering coefficient, and orbit. After generating the samples by simulating the reverse diffusion process, we quantize the entries of the adjacency matrices with the operator  $1_{x>0.5}$  to obtain the 0-1 adjacency matrix. Same as molecule generation, the encoder of HVAE equips 3 HGAT layers, and the decoder is a centroid-distance layer[21] followed by a shallow MLP. We fix the curvature of the hyperbolic space to -0.01 except Community-small, for which we set the curvature to -0.1. For score model  $s_\theta$ , we use HGAT layers to replace the GCN layers in GDSS[11]. We optimize all models with Riemannian Adam[64, 65]. We report the remaining hyperparameters used in the experiment in Table 6.

## B.3 Computing Resources

For all the experiments, we utilize PyTorch[66] to implement HGDM and train the score models on GeForce RTX 4090 GPU.

## C Visualization

In this section, we provide the visualizations of the graphs generated by our HGDM for the generic graph generation tasks and molecule generation tasks.

## C.1 Molecule Examples

We visualize a subset of molecules generated by HGDM in Figure 2 and 3.

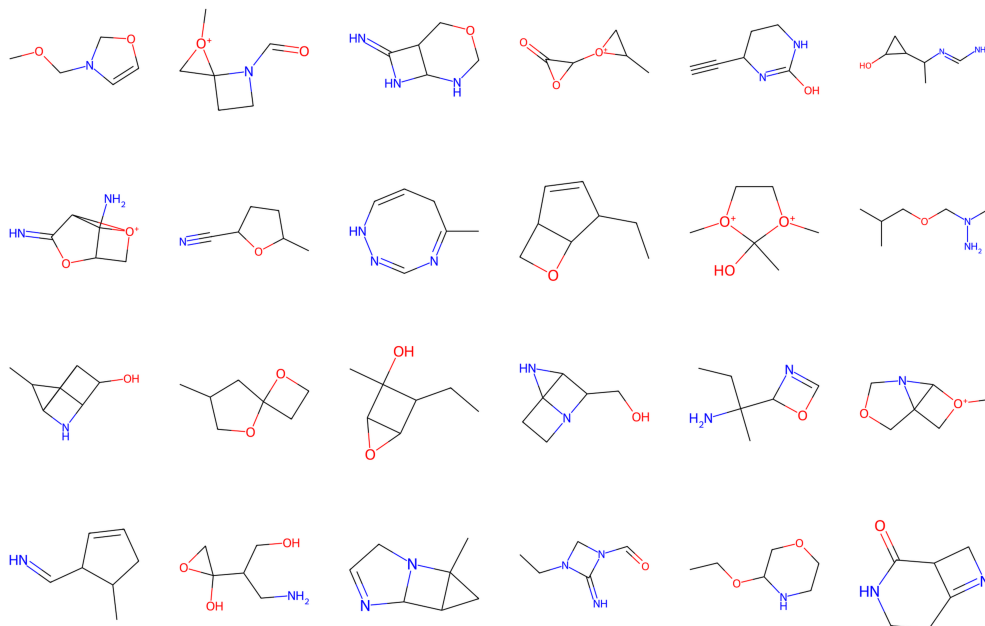


Figure 2: Random samples taken from the HGDM trained on QM9.

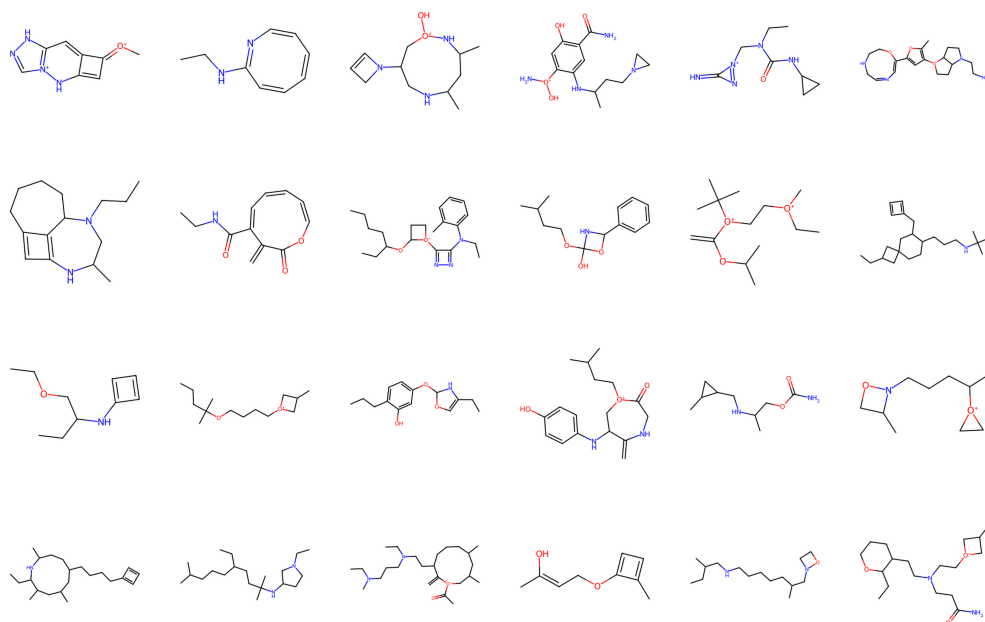


Figure 3: Random samples taken from the HGDM trained on ZINC250k.



## C.2 Generic Graph Examples

We visualize the graphs from the training datasets and the generated graphs of HGDM for each dataset in Figure 3-6. The visualized graphs are the randomly selected samples from the training datasets and the generated graph set. We additionally provide the information of the number of edges  $e$  and the number of nodes  $n$  of each graph.

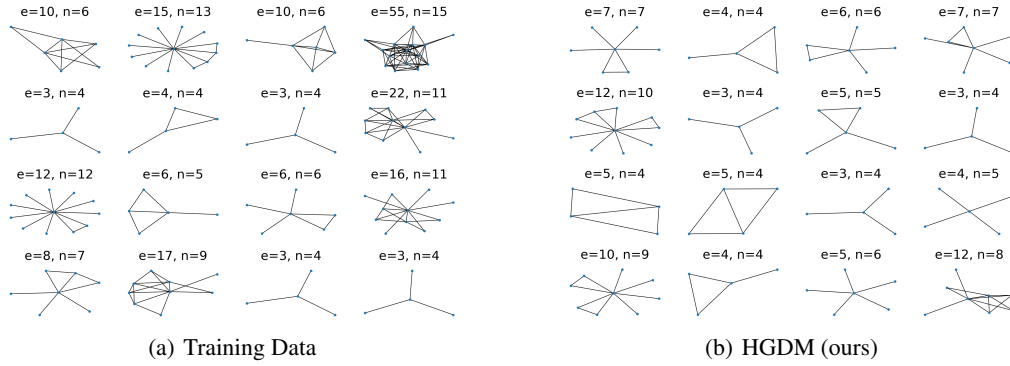


Figure 4: Visualization of the graphs from the Ego small dataset and the generated graphs of HGDM.

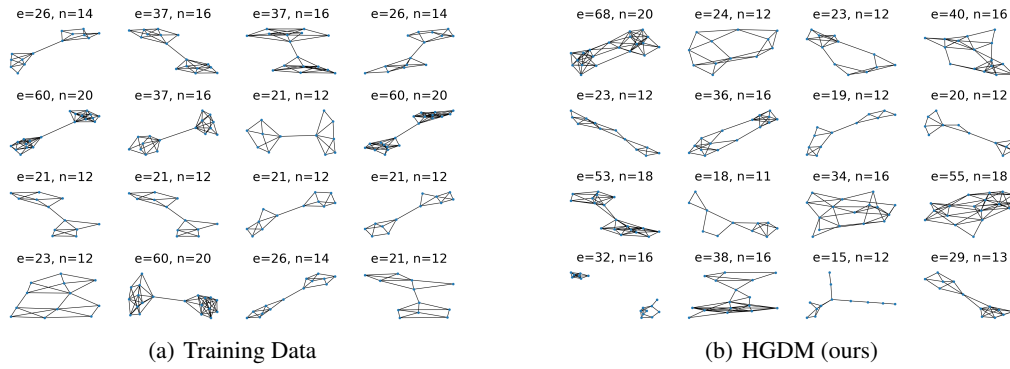


Figure 5: Visualization of the graphs from the Community small dataset and the generated graphs of HGDM.

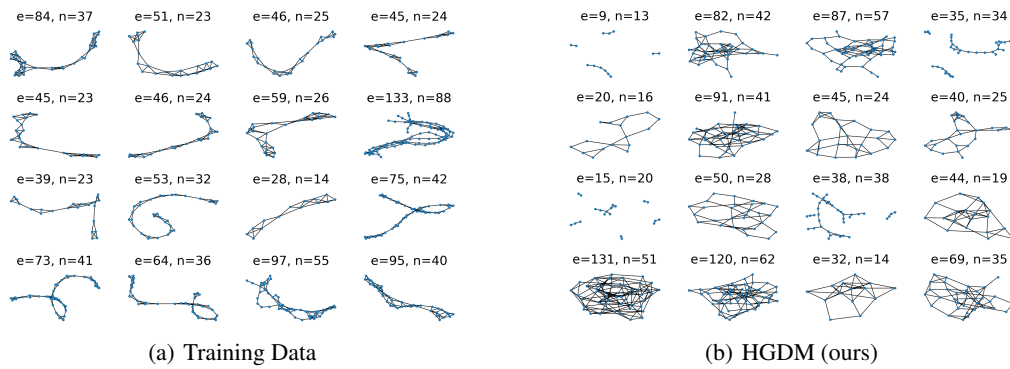


Figure 6: Visualization of the graphs from the Enzymes dataset and the generated graphs of HGDM.

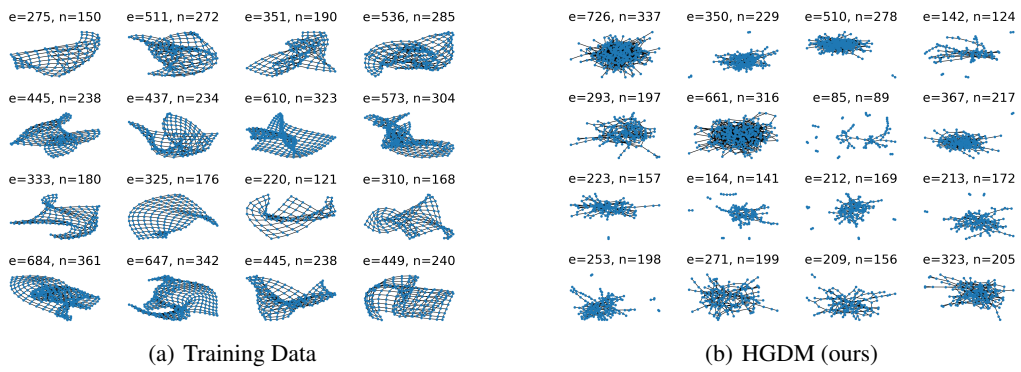


Figure 7: Visualization of the graphs from the Grid dataset and the generated graphs of HGDM.